J Electroceram (2008) 21:29–33
DOI 10.1007/s10832-007-9070-1

Solubility of silver in non-stoichiometric barium titanate

Wei-Hsing Tuan · Yen-Wei Cheng · Yung-Ching Huang

Published online: 14 March 2007

Abstract Barium titanate ($BaTiO_3$) can form solid solution with many oxides. The present study demonstrates that $BaTiO_3$ can also dissolve a small amount of Ag during co-firing, and its solubility depends strongly on the Ba/Ti ratio. A solid-state reaction was employed in the present study to prepare the $BaTiO_3$ powders with Ba/Ti ratio varied from 0.991 to 1.010. Fine Ag particles were then mixed intimately with the non-stoichiometric $BaTiO_3$ powders. The solubility of Ag in the non-stoichiometric $BaTiO_3$ at 1,350 and 1,390 °C was then determined by using a modified electron-probe micro-analysis (EPMA) technique. The solubility of Ag in Ti-rich $BaTiO_3$ is nearly double that in Ba-rich $BaTiO_3$. The diffusion distance of Ag in the non-stoichiometric $BaTiO_3$ is longer than 5 μm.

Keywords $BaTiO_3$ · Ag electrode · Solubility · Sintering

1 Introduction

Barium titanate ($BaTiO_3$) is a ferroelectric material with a perovskite structure. It can form solid solution with many ions [1]. The properties of $BaTiO_3$ can thus be modified through the solution with various ions. The $BaTiO_3$-based materials therefore exhibit versatile properties and many useful applications. For examples, $BaTiO_3$-based materials have been used for multilayer ceramic capacitors (MLCC) and positive temperature coefficient resistors (PTCR).

W.-H. Tuan (✉) · Y.-W. Cheng · Y.-C. Huang
Department of Materials Science and Engineering,
National Taiwan University, Taipei 106, Taiwan
e-mail: tuan@ccms.ntu.edu.tw

The solubility of a dopant in $BaTiO_3$ depends not only on the charge and radius of the dopant, it also shows strong dependence on the Ba/Ti ratio [1]. Silver or its alloys are frequently used as the inner and outer electrodes for MLCC components. The thickness of dielectric layer in MLCC is significantly reduced in the last decade. The interaction between electrode and dielectric could overshadow the performance of $BaTiO_3$-based dielectric. Recent studies demonstrated that a small amount of Ag could solution into $BaTiO_3$ during co-firing [2, 3]. However, the solubility of Ag in $BaTiO_3$ is low, and it imposes challenges on its measurement. Several techniques have been employed to determine the solubility of Ag in dielectrics [2–5]. The most popular analysis techniques involve the measurement of the Curie temperature [4, 5] and lattice parameter [3, 5]. However, the Curie temperature of dielectric is affected by many factors, such as the presence of internal stress, external stresses, microstructural characteristics [6] and Ba/Ti ratio [7]. The variation of the lattice parameter is small for the case that the solubility is low. For examples, Ikushima & Hayakawa claimed no change in the lattice parameter of their Ag-doped $BaTiO_3$; [4] Byrne and Cann did not detect any Ag solubility in the stoichiometric and BaO-excess $BaTiO_3$ by using this method [3].

A modified electron probe micro-analysis (EPMA) technique has been employed recently to determine the solubility of Ag or Pd in a Ti-rich $BaTiO_3$ [2]. The technique first places the electron probe on one Ag inclusion. Spot analysis is then carried out across the entire inclusion into the matrix. The EMPA usually collects the information not only from the surface but also from a volume under it. The radius of the volume is around 1 μm. If the spots are taken every 1 μm from the inclusion, the intensity of solute is high as one or more than one inclusion are present within the volume under the electron-probe. The

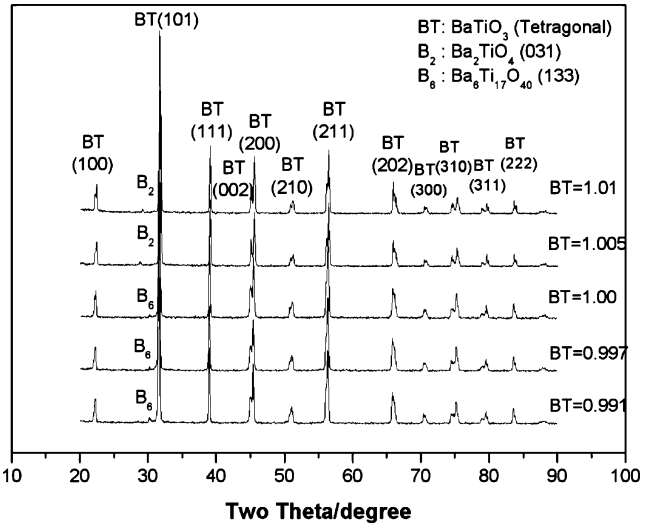

Fig. 1 XRD patterns for the non-stoichiometric $BaTiO_3$ after sintering at 1,350 °C

intensity then reduces to a plateau, when no more inclusion is detected. The height of the plateau thus indicates the solubility of the solute. The intensity can reduce to zero whenever the solubility is below the detection limit. The bonus of the technique is that the width of the plateau can be treated as the diffusion distance of the solute in matrix.

In the present study, the non-stoichiometric $BaTiO_3$ powders are prepared first. Fine Ag particles are then mixed intimately with the non-stoichiometric $BaTiO_3$ powders and co-fired at elevated temperature. The solubility of Ag in the non-stoichiometric $BaTiO_3$ is then determined with the modified EPMA technique.

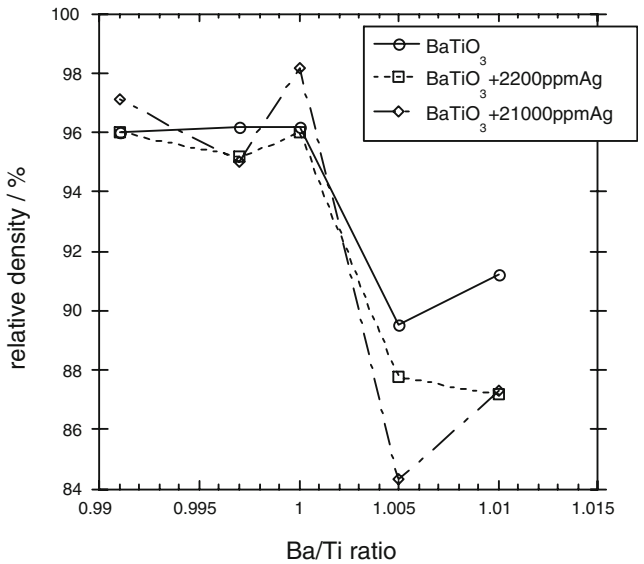

Fig. 2 Relative density of the Ag-doped non-stoichiometric $BaTiO_3$ specimens after sintering at 1,350 °C for 2 h

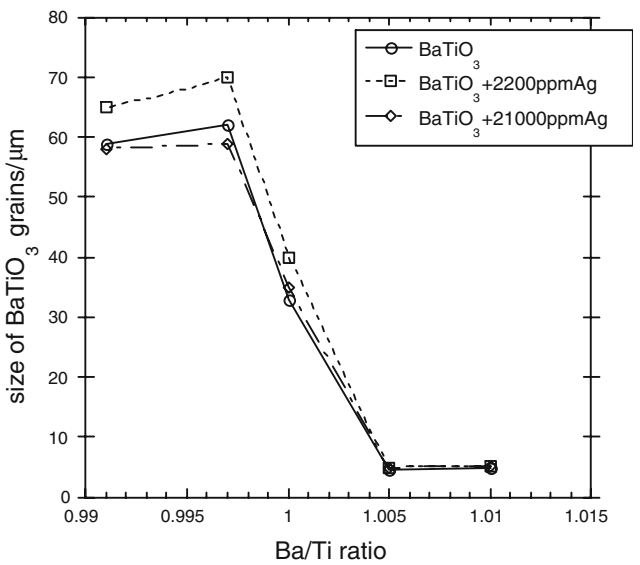

Fig. 3 Size of $BaTiO_3$ grains in the Ag-doped non-stoichiometric $BaTiO_3$ specimens as a function of Ba/Ti ratio. The specimens were sintered at 1,350 °C

2 Experimental

The $BaTiO_3$ powders with the Ba/Ti ratio varies from 0.991 to 1.010 were prepared by a solid-state reaction process. Various amount of $BaCO_3$ (BW-KLA, SAKAI Chem. Ind. Co., Ltd., Tokyo, Japan) and TiO_2 (High purity titanium dioxide, Toho Titanium Co., Ltd., Tokyo, Japan) powders were mixed with a turbo mixer in ethyl alcohol, using zirconia media, for 4 h. After drying, the powder mixtures were calcined at 1,100 °C for 2 h. The calcined powders were milled again to remove agglomerates. A laser particle size analyzer (Master 2000, Malvern Co., USA) was used to determine the particle size of the powders.

The non-stoichiometric $BaTiO_3$ powders were then mixed with 2,200 or 21,000 ppm (atoms of Ag per million formula units of $BaTiO_3$) Ag by using $AgNO_3$ as the starting sources. The powder mixtures were milled for 4 h, then left un-stirred at 30 °C for another 24 h. The slurry was dried and sieved with a #150 plastic mesh. The calcination was carried out at 300 °C for 24 h. The calcined powder mixtures were then sieved again. The powder compacts with 10 mm diameter and ~3 mm thickness were formed by applying a uniaxial pressing at 20 MPa. Two sintering temperatures, 1,350 and 1,390 °C, were used. The dwell time was 2 h, the heating rate 3 °C/min and the cooling rate 5 °C/min.

Silver could vaporize during co-firing [8], a surface layer ~0.5 mm thick was first removed from the sintered specimens, using SiC sandpaper, before all subsequent measurements. The final density was determined using the Archimedes method. Because the solubility of Ag in $BaTiO_3$ was low, as demonstrated later, the theoretical

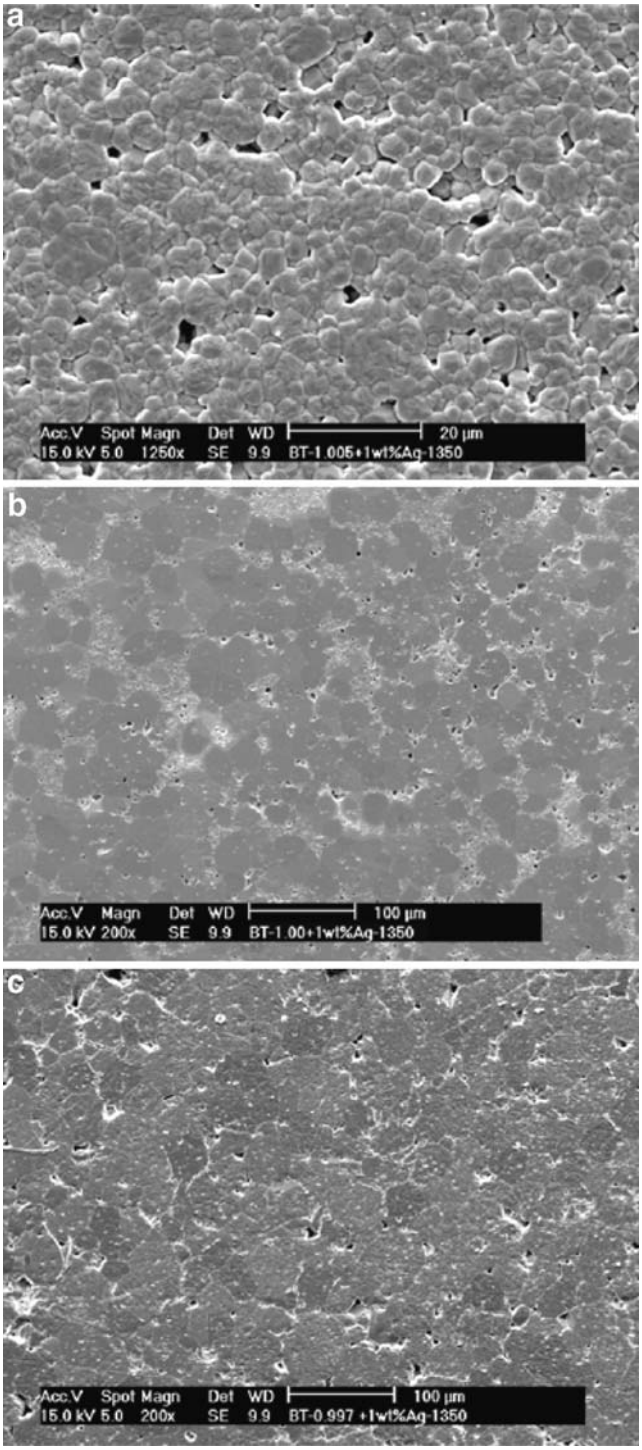

Fig. 4 Typical micrographs of Ag-doped Ba/Ti (**a**)~1.005, (**b**) 1.000 and (**c**) 0.997 $BaTiO_3$ specimens after sintering at 1350 °C.

density of the silver-doped $BaTiO_3$ was estimated using 6.02 g/cm [3] for $BaTiO_3$ and 10.50 g/cm^3 for Ag. The polished surface was prepared by grinding with SiC particles and polishing with Al_2O_3 particles. Grain boundaries were revealed by thermal etching at 1,250 °C for 0.5 h. The microstructure was observed by scanning electron microscopy (SEM). Phase identification was performed using X-ray diffractometry (XRD).

An EPMA-WDS (electron probe microanalyzer—wavelength dispersive spectrometry, Model JAX-8600SX, JEOL, Tokyo, Japan) facility was used under the operation conditions of 15 kV and 1×10^{-7} A, which resulted in an electron probe with the size of 1.5 μm. The detection limit of the facility, depending on the element, is <100 ppm after calibration with standard specimens. The specimens were polished only before the EPMA measurement. An un-doped $BaTiO_3$ specimen was used as a reference. One Ag inclusion within the non-stoichiometric $BaTiO_3$ matrix was located first, and then the electron probe was spotted every one micrometer along a straight line from the chosen inclusion. Approximately 20 points were taken for each scanned line. For each composition, around five scanned lines (~100 points) were chosen randomly from the polished surface.

3 Results and discussion

The XRD analysis reveals only $BaTiO_3$ phase in the powders after calcinations at 1,100 °C. The average particle size of the solid-state reacted powders is ~3 μm, the size of the non-stoichiometric $BaTiO_3$ powders is close to each other. Figure 1 shows the XRD patterns of the non-stoichiometric $BaTiO_3$ specimens after sintering at 1,350 °C for 2 h. A small amount of $Ba_6Ti_{17}O_{40}$ (B6) phase is detected in the Ba/Ti=0.991 and 0.997 sintered specimens, indicating that the Ba/Ti=0.991 and 0.997 specimens are rich in TiO_2 [9]. For the Ba/Ti=1.00 specimen, a very small amount of B6

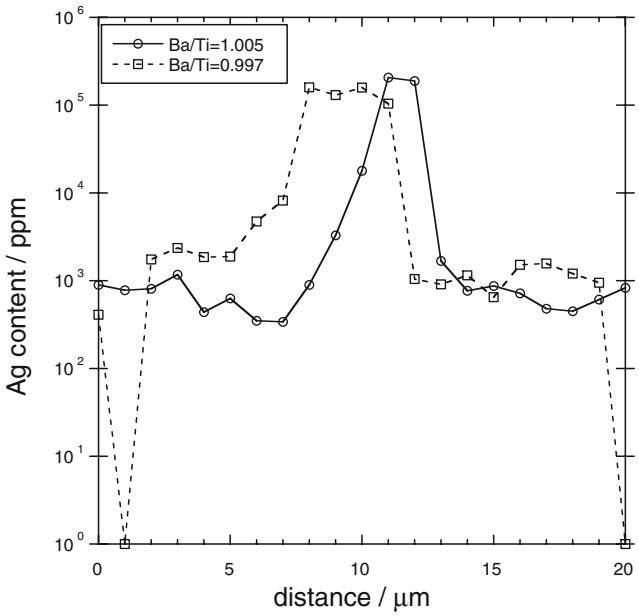

Fig. 5 One typical EPMA curve for a 21,000 ppm Ag-doped $BaTiO_3$ specimen. The specimen is sintered at 1,350 °C, the Ba/Ti ratio is 1.00

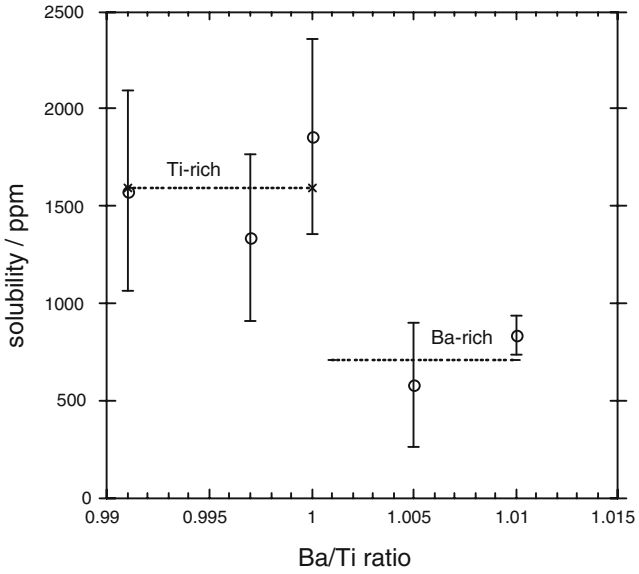

Fig. 6 Solubility of Ag in $BaTiO_3$ at 1,350 °C as a function of Ba/Ti ratio

phase is also found, suggesting that the Ba/Ti=1.00 specimen is also slightly rich in TiO_2. A small amount of Ba_2TiO_4 (B2) phase is detected in the Ba/Ti=1.005 and 1.010 specimens, suggesting that Ba/Ti=1.005 and 1.010 powders are rich in BaO.

Figure 2 shows the relative density of the non-stoichiometric $BaTiO_3$ specimens after sintering at 1,350 °C. The density of the Ba/Ti=0.991, 0.997, 1.00 specimens is higher than that of the Ba/Ti=1.005 and 1.010 specimens. Figure 3 shows the average size of $BaTiO_3$ grains in the non-stoichiometric $BaTiO_3$. Abnormal grains can be found only in Ba/Ti=0.991, 0.997, 1.00 specimens. The presence of the B2 phase could refine the microstructure of $BaTiO_3$ specimens [10]; the size of the $BaTiO_3$ grains in the Ba/Ti=1.005 and 1.010 specimens is therefore small. The excess TiO_2 can induce the formation of a liquid phase during sintering at a temperature higher than 1,332 °C [9]. The presence of the liquid phase enhances the densification and coarsening of $BaTiO_3$ during sintering, as demonstrated in Figs. 2 and 3.

The solid-state reaction technique is a straightforward technique to prepare the non-stoichiometric $BaTiO_3$ powders. Though extra care was taken to control the ratio of starting $BaCO_3$ and TiO_2 powders; a small amount of $BaCO_3$ may dissolve into water [11] (there is a small amount of water in the ethyl alcohol) or vaporize during sintering [12]. The Ba/Ti=1.00 specimen is thus slightly rich in TiO_2. The XRD and microstructure analyses are consistent to each other, they all suggest that the Ba/Ti=0.991, 0.997 and 1.00 specimens are rich in Ti, and Ba/Ti=1.005 and 1.010 specimens are rich in Ba.

Figure 4 shows typical micrographs of the Ag-doped non-stoichiometric $BaTiO_3$ specimens. The amount of Ag addition is low, and the particles are very small. The presence of the Ag particles shows minor influence on the densification behavior and microstructure of the non-stoichiometric $BaTiO_3$ specimens, Figs. 2 & 3. The densification behavior and microstructural development of the Ag-doped non-stoichiometric $BaTiO_3$ specimens are mainly dominated by the Ba/Ti ratio. It demonstrates the importance of Ba/Ti ratio on the density and microstructure of the $BaTiO_3$-based materials.

The EPMA analysis reveals no Ag signal in the non-stoichiometric $BaTiO_3$ specimens. Two typical EPMA patterns for the Ag-doped $BaTiO_3$ are shown in Fig. 5. By collecting only the data on the plateau, the solubility of Ag in $BaTiO_3$ (Fig. 6) is estimated. For the specific cases (Ba/Ti=1.05 and 0.997) shown in the figure, the solubility is, respectively, 690±230 and 1,400±500 ppm. The Ag intensity may drop to zero within the length of the scanned line, suggesting that the diffusion distance of Ag in the $BaTiO_3$ specimen at 1,350 °C is longer than 5 μm. Only very few Ag inclusions can be found in the 2,200 ppm Ag-doped specimens. Therefore, the EPMA analysis was mainly conducted by using the 21,000 ppm Ag-doped non-stoichiometric $BaTiO_3$ specimens. In any case, for the limited measurement on the 2,200 ppm Ag-doped specimens, the solubility value is close to that of the 21,000 ppm Ag doped $BaTiO_3$ specimens. It demonstrates that the EPMA technique used in the present study can deliver reliable estimation on the solubility of Ag in $BaTiO_3$. Table 1 summarizes the solubility of Ag in $BaTiO_3$ for the Ag-doped specimens after sintering at 1,350 °C. The results for the specimens sintered at 1,390 °C are also shown in the table. From the table, the solubility of Ag in $BaTiO_3$ increases with the increase of co-firing temperature; furthermore, the solubility of Ag in the Ti-rich specimen

Table 1 Solubility of Ag in the non-stoichiometric $BaTiO_3$ sintered at 1,350 or 1,390 °C.

Cofiring temperature	Ba/Ti ratio	~1.010	~1.005	~1.000	~0.997	~0.991
1,350 °C	Solubility/ppm[a]	840±100	580±320	1,860±500	1,340±430	1,580±520
	Diffusion distance/μm	~5	~5	>8	>9	>9
1,390 °C	Solubility/ppm[a]	1,500±500	750±400	2,300±1,200	3,000±1,000	3,700±1,700
	Diffusion distance/μm	>6	>8	>6	>8	>6

[a] atoms of impurity per million formula units of $BaTiO_3$.

is higher than that in the Ba-rich specimen. The Ag ion can diffuse a distance longer than 5 μm at a temperature higher than 1,350 °C, Table 1. The table clearly demonstrate that Ag can diffuse into every grain within two Ag electrodes, as the dielectric thickness is less than 10 μm.

The solubility of BaO and TiO_2 in $BaTiO_3$ at 1,300 °C is <100 and ~300 ppm, respectively [14]. The excess BaO can form titanium vacancy and oxygen vacancy in $BaTiO_3$ as [13, 15]

$$BaO \overset{BaTiO_3}{\rightarrow} V_{Ti}^{''''} + Ba_{Ba} + O_o + 2V_o^{\bullet\bullet} \quad (1)$$

Apart from the formation of a liquid phase at elevated temperature, excess TiO_2 can also induce the formation of barium vacancy and oxygen vacancy in $BaTiO_3$ as [12, 14]

$$TiO_2 \overset{BaTiO_3}{\rightarrow} V_{Ba}^{''} + Ti_{Ti} + 2O_o + V_o^{\bullet\bullet} \quad (2)$$

Though the valence of Ag ion is smaller than that of Ba ion (+1 vs. +2), the ionic radius of Ag ion is close to that of Ba ion (0.149 vs. 0.135 nm), Ag ion thus tends to substitute Ba ion. Our previous study found that the solubility of Ag in $BaTiO_3$ decreases with the decrease of oxygen partial pressure [2], suggesting that Ag ion acts as acceptor to $BaTiO_3$. The incorporation of Ag acceptor is accompanied by the formation of oxygen vacancy as [2, 3]

$$Ag_2O \overset{BaTiO_3}{\rightarrow} 2Ag_{Ba}^{'} + O_o + V_o^{\bullet\bullet} \quad (3)$$

Apart from the valence difference between Ag ion and Ba ion, the solution of Ag acceptor induces the formation of oxygen vacancy, which is relatively abundant within both Ti-rich and Ba-rich $BaTiO_3$. The reaction 3 is thus not chemically favorable. The solubility of Ag in $BaTiO_3$ is therefore low. Since Ag ion tends to replace Ba ion, the presence of Ba vacancy is favorable for the solution of Ag ion. Therefore, the solubility of Ag in Ti-rich specimen is therefore higher than that in the Ba-rich specimen.

The defect chemistry is usually applied to analyze the defect concentration within the lattice. The EPMA technique employed in the present study collects the information within a volume of more than 1 μm [3]. The technique gives the average value within the volume. The defect chemistry can thus be used to estimate the defect change associated with the Ag addition. However, the dopant concentration at the grain boundary may be higher, and its diffusion distance along the grain boundary may be longer. The EPMA technique could not estimate these contributions. However, though the grain size in the Ba-rich specimens is much smaller than that in the Ti-rich specimens; the solubility of Ag is lower in the Ba-rich $BaTiO_3$. It further confirms that the trend on the solubility estimated by the present EPMA technique is correct.

4 Conclusions

In the present study, the Ba-rich and Ti-rich $BaTiO_3$ powders are first prepared by using a solid-state reaction process. The solubility of Ag in the non-stoichiometric $BaTiO_3$ is then measured by using an EPMA technique. The Ba-rich and Ti-rich $BaTiO_3$ can all dissolve a small amount of Ag. The solubility of Ag in the Ti-rich $BaTiO_3$ is around 1,600 and 3,000 ppm at 1,350 and 1,390 °C, respectively. The Ag solubility in Ba-rich $BaTiO_3$ is around 700 and 1,100 ppm at 1,350 and 1,390 °C, respectively. The diffusion distance of Ag in $BaTiO_3$ is longer than 5 μm, indicating that the Ag acceptors are likely always present in the $BaTiO_3$-based dielectric as its thickness is smaller than 10 μm and co-fired with Ag electrode at elevated temperature.

Acknowledgment The present study is supported by the National Science Council, Taiwan, R.O.C., through Contract no. NSC92-2216-E-002-029.

References

1. D. Makovec, Z. Samardzija, M. Drofenik, J. Am. Ceram. Soc. **87**, 1324 (2004)
2. S.J. Shih, W.H. Tuan, J. Am. Ceram. Soc. **87**, 401 (2004)
3. T.A. Byrne, D.P. Cann, J. Am. Ceram. Soc. **87**, 875 (2004)
4. H. Ikushima, S. Hayakawa, Jpn. J. of Appl. Phys. **4**, 328 (1965)
5. Y. Sato, H. Kanai, Y. Yamashita, J. Am. Ceram. Soc. **79**, 261 (1996)
6. H.J. Hwang, T. Nagai, T, Ohji, M. Sando, M. Toriyama, K. Niihara, J. Am. Ceram. Soc. **81**, 709 (1998)
7. K. Sakayori, Y. Matsui, H. Abe, E. Nakamura, M. Kenmoku, T. Hara, D. Ishikawa, A. Kokubu, K. Hirota, T. Ikeda, Jpn. J. Appl. Phys. **34**, 5443 (1995)
8. C.Y. Chen, W.H. Tuan, J. Am. Ceram. Soc. **83**, 2988 (2000)
9. B.-K. Lee, S.-Y. Ching, S.-J.L. Kang, Acta Mater. **48**, 1575 (2000)
10. F. Kulcsar, J. Am. Ceram. Soc. **39**, 13 (1959)
11. K.W. Kirby, B.A. Wechsier, J. Am. Ceram. Soc. **74**, 1841 (1991)
12. C.-C. Li J.-H. Jean, J. Am. Ceram. Soc. **85**, 2977 (2002)
13. J.-S. Chun, N.-M. Hwang, D.-Y. Kim, J. Am. Ceram. Soc. **87**, 1779 (2004)
14. J.H. Hwang, Y.H. Han, Electrochemistry **68**, 423 (2000)
15. N.-H. Chan, R.K. Sharma, D.M. Smyth, J. Am. Ceram. Soc. **64**, 556 (1981)